CHAPTER 10.19

Aqueous-Phase Redox Precipitation

Courtney A. Young and Hsin-Hsiung Huang

Precipitation is a commonplace, hydrometallurgical process used to synthesize metal-bearing solids from solution. It is accomplished by the various techniques shown in Figure 1, which is similar to the original illustration presented by Habashi (1999). As indicated, these techniques are classified as either physical or chemical precipitation and are described elsewhere in this handbook. In general, the techniques on the left tend to be heterogeneous reactions that are used to produce compounds, and those on the right tend to be homogeneous reactions that are usually used to make metal. They are briefly reviewed here to set the stage for discussing aqueous-phase reduction–oxidation (redox) precipitation.

In physical precipitation, also known as crystallization, cooling and/or evaporation are used to make compounds normally in the absence of chemical addition. By comparison, chemical precipitation is accomplished by adding reagents, thereby inducing one of four processes: hydrolytic, ionic, substitution, and redox precipitation. These four processes are also used to yield compounds; however, redox precipitation is more commonly used to produce metal. For example, hydrolytic precipitation is primarily used to make compounds as hydroxides (OH^-) and oxides (O^{2-}) by simply adjusting the solution pH. Although hydrolytic precipitation is a form of ionic precipitation, the latter generally refers to compounds precipitated upon addition of sulfides (S^{2-}), halides (e.g., F^- and Cl^-), and oxyanions (e.g., SO_4^{2-}, CO_3^{2-}, and PO_4^{3-}) among many other anions. Likewise, substitution precipitation occurs when ligands, including waters of hydration, are coordinated with a transition metal and are displaced by other ligands, causing the transition metal to precipitate. Such reactions are dependent on coordination chemistry and ligand size. Substitution precipitation often occurs when one or more cations are precipitated by one or more anions, yielding either a compound in stoichiometric proportion such as a double salt (as is often the case for cyanide, CN^-) or in nonstoichiometric composition such as a solid solution (as is often the case for silicates, SiO_4^{2-}). Finally, in redox precipitation, a change in oxidation state occurs, requiring electrons to be transferred either electrolytically or electrochemically in a process typically used to make metal.

With electrolytic precipitation, an electrical current is supplied externally via batteries, generators, and power plants, depending on the scale needed. Electrowinning and electrorefining are used almost exclusively for metal reduction. Electron transfer can also be done internally via electrochemical reactions involving solid, gas, and aqueous phases. Solid-phase redox precipitation is predominantly used as a reductive process more commonly referred to as cementation. Gas-phase redox precipitation is also predominantly reductive and is exemplified with the use of hydrogen. With aqueous-phase redox precipitation, ionic and nonionic species are dissolved in solution and used as either oxidants or reductants. Because solid- and gas-phase reactions involve solid and gas phases as reactants, they are heterogeneous. By comparison, when the reactants are all dissolved species, the electrochemical reactions are homogeneous.

In the literature, emphasis has predominantly been on "ionic" reductive precipitation; however, this terminology does not apply to similar reactions involving nonionic species as well as oxidative precipitation. Furthermore, this terminology is easily confused with "ionic" chemical precipitation where redox reactions do not occur. Consequently, in keeping with the names of solid- and gas-phase redox precipitation, it is more appropriately referred to herein as aqueous-phase redox precipitation. Hence, this chapter examines several ionic and nonionic redox precipitation processes, including organic reactants. Example thermodynamic calculations using StabCal software (Huang 2018) are illustrated with E_H–pH (Pourbaix) diagrams for selected case studies. Thermodynamic data were predominantly taken from the National Bureau of Standards (NBS; Wagman 1982); however, data taken from other sources were made consistent to the NBS data so calculation errors would be prevented. The sources are identified within as needed. Additional case studies are also presented to demonstrate aqueous-phase redox precipitation for other metals, but associated E_H–pH diagrams are not presented, to minimize duplication.

Courtney A. Young, Department Head & Professor, Metallurgical & Materials Engineering, Montana Tech, Butte, Montana, USA
Hsin-Hsiung Huang, Professor, Department of Metallurgical & Materials Engineering, Montana Tech, Butte, Montana, USA

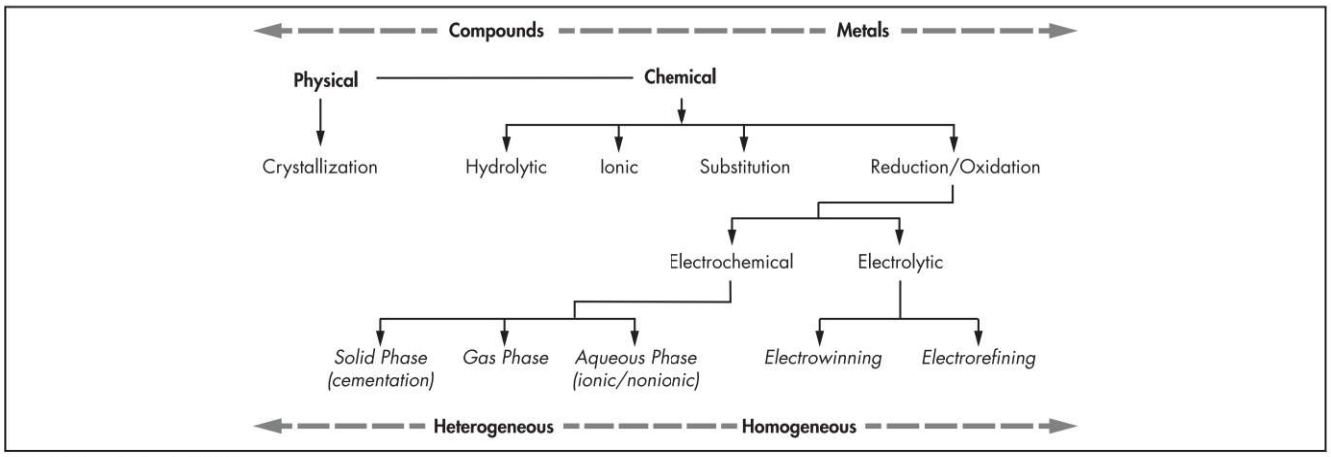

Adapted from Habashi 1999

Figure 1 Types of precipitation processes used in hydrometallurgy

INDUSTRIAL AND LABORATORY PRACTICES

Aqueous-phase redox precipitation is essentially no different than traditional precipitation. Reactions are therefore conducted in the same vessels conducted in either batch or continuous-flow mode. Reactors would therefore include but not be limited to stirred tanks/mixers/agitators, thickeners/clarifiers, tube/pipe reactors, airlifts/bubble columns, crystallizers, fluidized beds, and filter chambers. Two issues may need to be addressed to improve reaction efficiencies. First, potential control may be necessary such that, for example, solutions can be deaerated to remove dissolved oxygen, particularly in the case when aqueous-phase reduction is being done. Reactors may therefore need special features to allow this or be preceded with a conditioning tank where it is done. Second, as is the case for all precipitation vessels, special consideration may be needed for solid–liquid separation to remove the precipitate from the solution. This is done simultaneously with filter chambers and thickeners/clarifiers. It can also be aided by seeding the precipitate so that large particles are obtained and/or by using vessels with appropriate designs, as exemplified with inward or outward flows on stirred-tank reactors.

GENERAL THEORY

Redox Reactions

Because electrochemical reactions involve changes in oxidation state, they can be represented as half-cell reactions to illustrate the electron transfer that occurs. In this regard, a principal goal of hydrometallurgical processing is to precipitate the metal (M°) of interest from its cation (M^{2+}) by reduction such that the reducing agent (R^{+}) simultaneously undergoes oxidation:

Cathodic reduction: $M^{2+} + 2e^{-} = M°$ **(EQ 1)**

Anodic oxidation: $R^{+} = R^{2+} + e^{-}$ **(EQ 2)**

Obviously, the two half-cell reactions are balanced regarding the number of electrons being transferred and then summed to yield the overall electrochemical process:

Redox reaction: $M^{2+} + 2R^{+} = M° + 2R^{2+}$ **(EQ 3)**

Thus, in this case, two dissolved species electrochemically react to precipitate the more noble metal. It is preferred that the other product (R^{2+}) does not precipitate and therefore remains in solution or is evolved off as a gas.

Butler–Volmer Equations

Because electrode kinetics can be used to model these reactions, the Butler–Volmer equations for the cathodic and anodic reactions apply. To illustrate, the theoretical redox couple, R^{+}/R^{2+}, used in Equations 2 and 3 is exemplified:

Cathodic reduction ($R^{2+} + e^{-} = R^{+}$):

$$i_c = i_o \exp[(-\alpha)nF\eta/RT] \quad \textbf{(EQ 4)}$$

Anodic oxidation ($R^{+} = R^{2+} + e^{-}$):

$$i_a = i_o \exp[(1-\alpha)nF\eta/RT] \quad \textbf{(EQ 5)}$$

where α is the transfer coefficient that is used as a measure of symmetry between the half-cell reactions of the redox couple; n is the number of electrons involved (mol); F is Faraday's constant (23,060 cal/V); R is the gas constant (1.986 cal/mol/K); T is temperature (K); i_c is the cathodic current (amp); i_a is the anodic current (amp); i_o is the exchange current (amp) at $\eta = 0$ and where $i_a = -i_c$; and η is the potential (V) difference ($E - E_{eq}$), such that E_{eq} is the equilibrium potential (V) determined from thermodynamics according to the Nernst equation and E is the measured or applied potential (V). Thus, +η is referred to as the overpotential and –η, the underpotential. By summing the cathodic and anodic currents, the total current results in the following:

Total faradic current: $i = i_c + i_a$ **(EQ 6)**

However, because each half-cell reaction involves dissolved species, they are dependent on concentration and will eventually become mass-transfer (diffusion) controlled. This occurs at undervoltages less than –η for the cathodic reaction and at overvoltages greater than +η for the anodic reaction. At these potentials, the limiting currents of $i_{l,c}$ and $i_{l,a}$ are reached for both half-cell reactions, respectively. All of these parameters are illustrated by the current–potential plot in Figure 2. By taking the log of the absolute values of i, i_c, and i_a, the Tafel plot shown in the inset at the bottom right of Figure 2 results.

Applying this concept to the cathodic reaction of the more noble metal (Equation 1) and the anodic reaction of

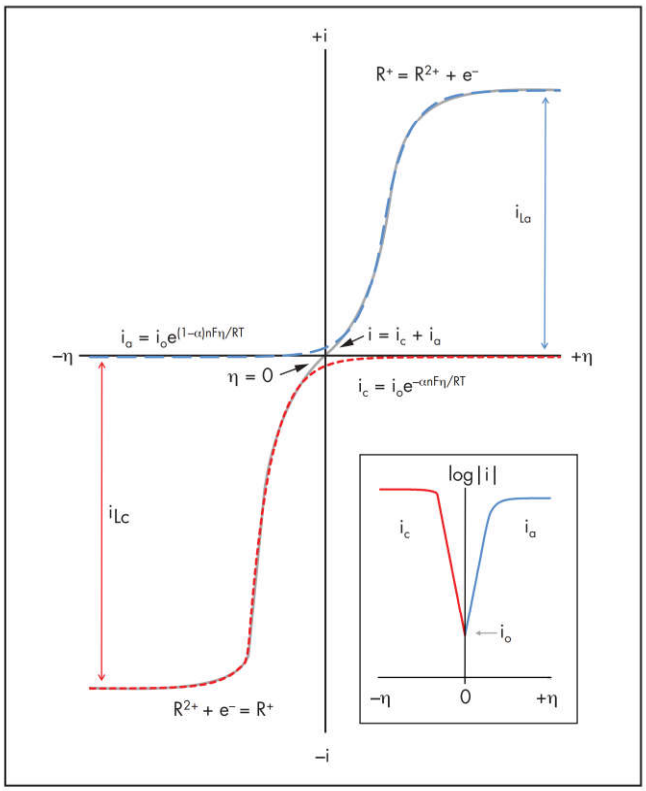

Figure 2 Current–potential plot of a theoretical redox couple R^{2+}/R^{+} (inset shows the resulting Tafel plot)

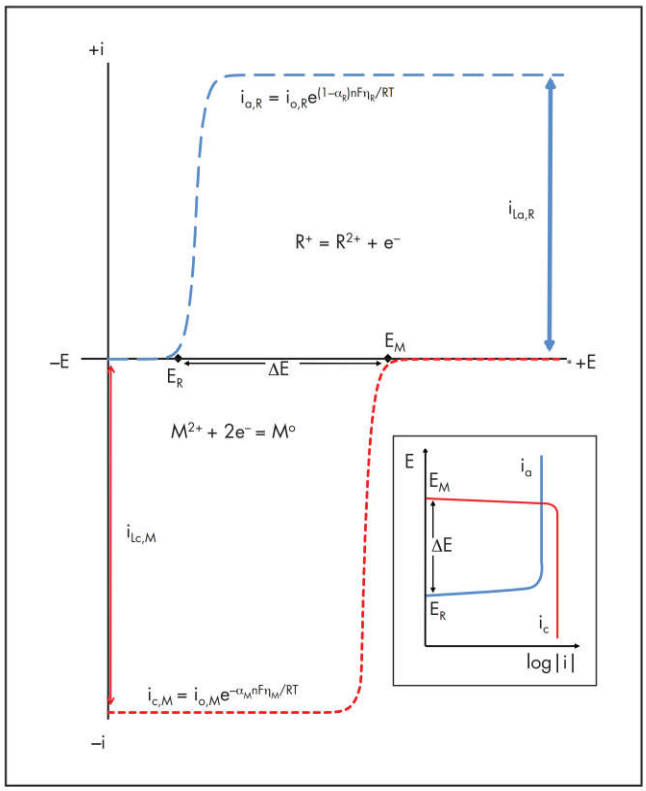

Figure 3 Current–potential plot of a theoretical redox precipitation reaction involving aqueous phases (inset shows the resulting Evans diagram)

the more reactive reductant (Equation 2) yields the current–potential plot in Figure 3. This causes the cathodic reaction in Figure 2 to shift to higher potentials, resulting in an overvoltage ($\eta = \Delta E = E_M\text{-}E_R$) that drives the redox reaction (Equation 3). As with cementation reactions, if this overvoltage exceeds approximately 0.36 V, the reaction is expected to become mass-transfer controlled, as determined by the half-cell reaction with the lower limiting current. The rate of the other half-cell reaction should then be chemically controlled. This is illustrated by the Evans diagram inset at the bottom right of Figure 3, which shows, in this example, mass transfer being controlled by the anodic oxidation reaction and chemical control by the cathodic reduction reaction.

While the overvoltage is critical, many other parameters play significant roles in the kinetics and include the faradic and exchange currents (i and i_o), temperature (T), reactant concentrations (R^+ and M^{2+}), product concentration (R^{2+}), and the charge of the dissolved species. The latter is not often considered in the literature, but, as exemplified in Reaction 3, if cations are reacting, repulsion forces between them will slow the reaction; however, if the reacting ions are oppositely charged, attractive forces should increase the reaction. Furthermore, if one reactant is neutral, it should not affect the reaction at all. Similar analogies can also be made regarding the dissolved products that form.

E_H–pH Diagrams

The beauty of redox reactions is that they can be illustrated with Pourbaix diagrams. Because these diagrams plot potential (E_H) as a function of pH, they are also referred to as E_H–pH diagrams. Like other speciation diagrams, they are determined from thermodynamic calculations to show which species are predominantly stable under particular conditions referred to as predominant stability regions. Furthermore, a line that separates two regions represents the conditions needed for a reaction to occur at equilibrium between the predominant species in the regions. Hence, E_H–pH diagrams show the predominant species and reactions with neighboring species under the influence of E_H and pH. However, the effects of temperature as well as ligand type and concentration can also be illustrated. To calculate a line, for example, the redox reaction and free energy of the reaction (dG_{rxn}) between species A and B undergoing redox change in the presence of two complexing ligands C and D are as follows:

$$\text{Redox reaction: } aA \leftrightarrow bB + cC + dD + hH^+ + ne^- \quad \textbf{(EQ 7)}$$

$$\text{Free energy: } dG_{rxn} = \Sigma(\nu_i \times dG_i^\circ) \quad \textbf{(EQ 8)}$$

where lowercase letters and ν_i represent the stoichiometric coefficients for each species from the reaction and, of course, H^+ is the hydrogen cation. Species shown on the left-hand side of the equation will have negative coefficients and vice versa. The letter n represents the number of electrons (e^-) involved, and dG_{rxn} relates to the reaction equilibrium constant and can be calculated from free energy of formation dG° of species with their stoichiometric coefficients. According to the Nernst equation for the redox reaction in Equation 7, the equilibrium between A and B is linear with $E_H = a + b \times pH$ and can be expressed as

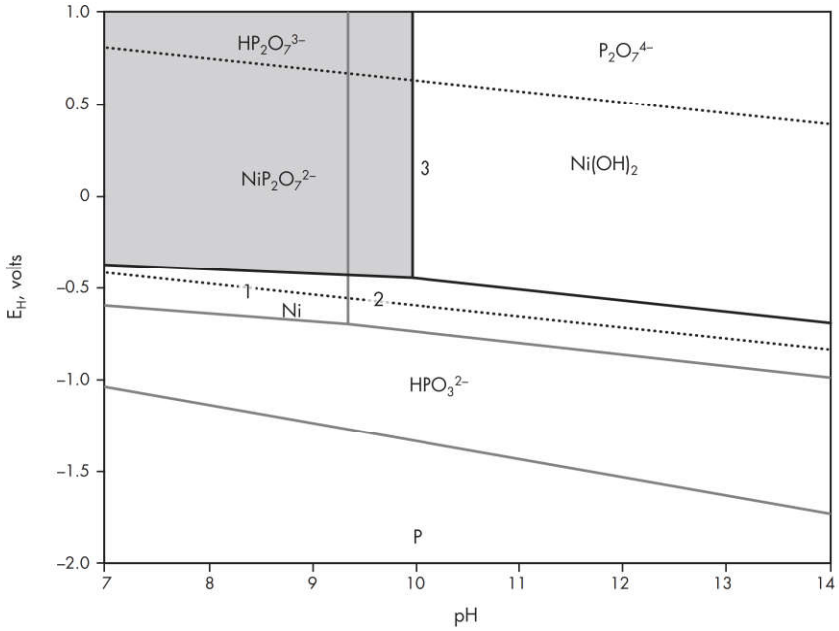

Note: Thermodynamic data are from Wagman 1982.

Figure 4 E_H–pH diagram of nickel illustrating the boundary lines between $NiP_2O_7^{2-}$ (in shaded area) and surrounding species (Ni and $Ni(OH)_2$) as influenced by P ligands of $HP_2O_7^{3-}$ and $P_2O_7^{4-}$ (labeled in gray)

Table 1 E_H–pH equations determined from thermodynamics for equilibrium reactions of $NiP_2O_7^{2-}$ with Ni and $Ni(OH)_2$

Line	Chemical Reaction	dG_{rxn}, kcal	E_H–pH Equation
1	$Ni(s) + HP_2O_7^{3-} \leftrightarrow 2e^- + NiP_2O_7^{2-} + H^+$	–7.696	$E_H = -0.17240 - 0.02958$ pH
2	$Ni(s) + P_2O_7^{4-} \leftrightarrow 2e^- + NiP_2O_7^{2-}$	–20.411	$E_H = -0.44809$
3	$2H^+ + Ni(OH)_2 + P_2O_7^{4-} \leftrightarrow NiP_2O_7^{2-} + 2H_2O$	–26.878	pH = 9.94439

$$E_H = E_H^\circ + \frac{\ln(10)RT}{(n \times F)}\left[\log\left(\frac{\{B\}^b\{C\}^c\{D\}^d}{\{A\}^a}\right)\right] - \frac{\ln(10)RT}{(n \times F)} \times hpH \quad \textbf{(EQ 9)}$$

where

$$E_H^\circ = \frac{dG_{rxn}}{(n \times F)}$$

and, for non-redox reactions between A and B where n = 0, the equation would be a vertical line at x = pH expressed as

$$pH = \frac{1}{h} \times \left\{-\log K + \left[\log\left(\frac{\{B\}^b\{C\}^c\{D\}^d}{\{A\}^a}\right)\right]\right\} \quad \textbf{(EQ 10)}$$

where

$$-\log K = \frac{dG_{rxn}}{\ln(10)RT}$$

such that {species} denotes the species activity and other terms are as defined previously. It is understood that solid species have unit activity and aqueous species have activities determined by the product of concentration in molarity (M) and an activity coefficient γ. It is understood that horizontal lines can also be determined for redox reactions in cases where h = 0.

To demonstrate, the E_H–pH diagram of nickel complexed with phosphorus at 25°C is shown in Figure 4 using the same conditions noted later in case study 1 (i.e., [P] = 0.40, [Ni] = 0.13 M, T = 298 K). The predominant area of $NiP_2O_7^{2-}$ (shaded) is complexed by $HP_2O_7^{3-}$ at lower pH and $P_2O_7^{4-}$ at higher pH. $NiP_2O_7^{2-}$ is also surrounded by two solids: Ni and $Ni(OH)_2$. The chemical reactions, free energies (dG_{rxn}), and resulting equations for $NiP_2O_7^{2-}$ in equilibrium with Ni and $Ni(OH)_2$ as affected by the different ligands are listed in Table 1. The equations match those highlighted in the figure.

ILLUSTRATED CASE STUDIES

Case Study 1—Ionic Reduction of Nickel

Electroless plating is one of the best examples of ionic reductive precipitation. The technology has been used on a variety of base and precious metals, including but not limited to Ni, Cu, Co, Au, Pt, Ag, and their alloys (Mallory and Hadju 1990). It was first developed by Brenner and Riddell (1946) for nickel plating on steel and has since been well studied and documented (Sudagar et al. 2013). In one example, Mallory (1990) examined and compared four reductants, namely, nonionic hydrazine (N_2H_4) and dimethylamine borane [$(CH_3)_2NHBH_3$] as well as ionic borohydrite (BH_4^-) and hypophosphite

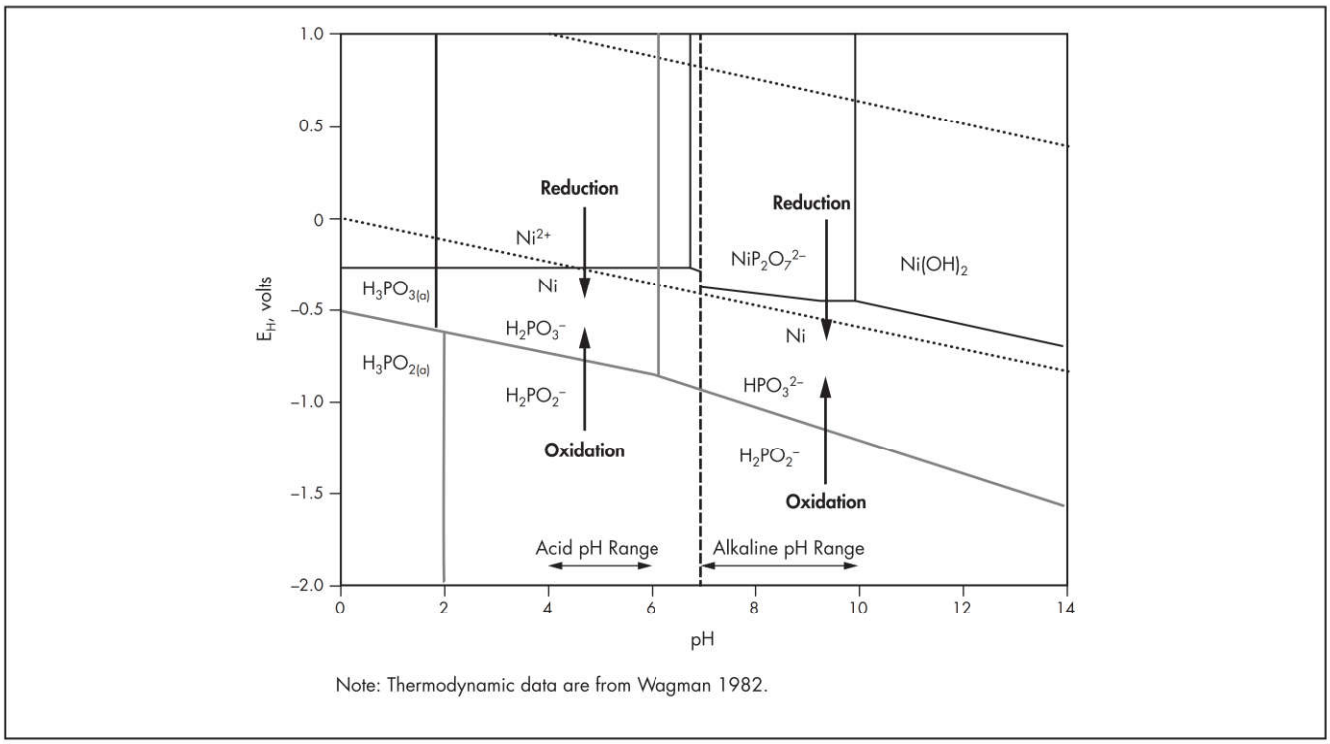

Figure 5 E_H–pH diagram for nickel electroless plating by hypophosphite ($H_2PO_2^-$) in acidic (left) and basic (right) conditions

($H_2PO_2^-$) with the following "primary" redox reactions occurring, respectively:

$$\text{Anodic reduction:} \quad Ni^{2+} + 2e^- = Ni° \qquad \textbf{(EQ 11)}$$

$$\text{Cathodic oxidation:} \quad N_2H_4 = N_2 + 4H^+ + 4e^- \qquad \textbf{(EQ 12)}$$

$$(CH_3)_2NHBH_3 + 3H_2O = (CH_3)_2NH_2^+ + H_3BO_3 + 5H^+ + 6e^- \qquad \textbf{(EQ 13)}$$

$$BH_4^- + 4H_2O = B(OH)_4^- + 8H^+ + 8e^- \qquad \textbf{(EQ 14)}$$

$$H_2PO_2^- + H_2O = H_2PO_3^- + 2H^+ + 2e^- \qquad \textbf{(EQ 15a)}$$

such that dimethylammonium [$(CH_3)_2NH_2^+$], boric acid (H_3BO_3), tetrahydroxyborate [$B(OH)_4^-$], and byphosphite ($H_2PO_3^-$) are also produced. However, the reductants also reduce water to hydrogen gas that, in turn, can react with the reductants themselves, causing, for example, elemental B and P to also precipitate out. These side reactions are ignored here so that the primary reactions can be easily illustrated with thermodynamics using StabCal (Huang 2018). In this case, hypophosphite is examined under acidic and basic conditions.

Acidic Hypophosphite

The resulting E_H–pH diagram at 298 K in Figure 5 (at the left) depicts the ionic reduction of 7.5 g/L Ni^{2+} by 25 g/L $H_2PO_2^-$, which are typical concentrations identified by Mallory (1990). The diagram shows that the best conditions for electroless plating are between pH 5 and 6 with the Ni° forming near –0.3 V and $H_2PO_3^-$ near –0.8 V. Because the reaction produces acid (Reactions 15a, 15b), it will likely be best at the higher pH with pH control; furthermore, the higher pH will also yield the greater potential difference (ΔE = 0.6 V) to help drive the reaction even more.

Alkaline Hypophosphite

At the right in Figure 5, the E_H–pH diagram also shows that nickel could be electrolessly plated under alkaline conditions. In this case, Ni^{2+} would exist as a diphosphate complex ($NiP_2O_7^{2-}$) and would undergo reduction to produce both metal and metaphosphite (HPO_3^-):

$$\text{Anodic reduction:} \quad NiP_2O_7^{2-} + 4H^+ + 6e^- = Ni° + 2HPO_3^{2-} + H_2O \qquad \textbf{(EQ 16)}$$

$$\text{Cathodic oxidation:} \quad H_2PO_2^- + H_2O = HPO_3^{2-} + 3H^+ + 2e^- \qquad \textbf{(EQ 15b)}$$

The half-cell reactions would occur near –0.4 V and –1.1 V, respectively. By comparison, the ΔE of 0.7 V is slightly higher and the reaction occurs in a wider pH range (7 to 10), making pH control easier. Side reactions would also occur, causing, for example, elemental P to form. In addition, hypophosphite ($H_2PO_2^-$) consumption would be three times greater.

Case Study 2—Inorganic Reduction of Gold

Reductive precipitation has been used historically for detecting the presence of metals, particularly gold (Au) and other precious metals. With this technology, a sample is often treated with aqua regia (1:3 ratio of HNO_3:HCl) at elevated temperature to solubilize any gold that may be present as gold chloride ($AuCl_4^-$). The resulting solution is then treated with inorganic chemicals like stannous chloride ($SnCl_2$) and ferrous sulfate ($FeSO_4$), resulting in a precipitate if gold is present. Today, this technology has been adapted to many reductants, with ionic inorganic compounds being emphasized in this case study and organic compounds in case study 3.

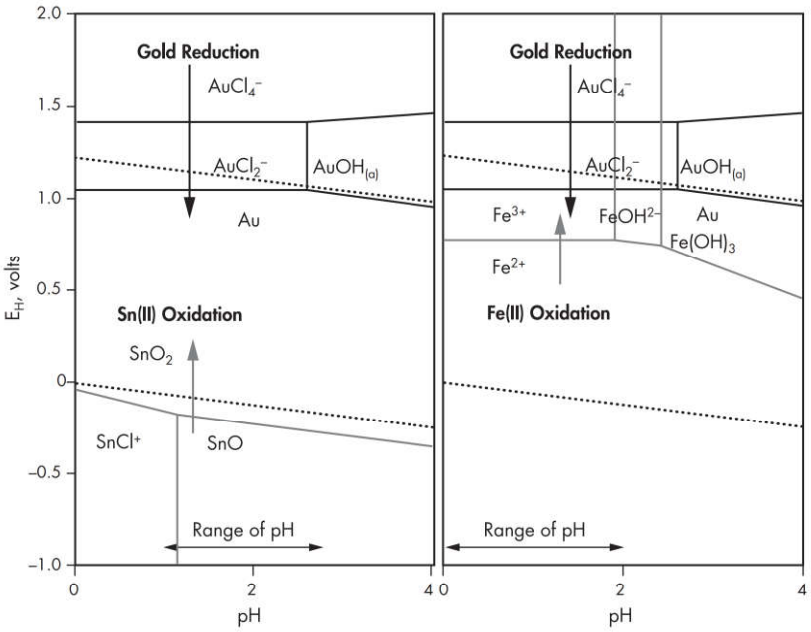

Note: Thermodynamic data are from Wagman 1982; Johnson et al. 1992; and House and Kelsall 1984.

Figure 6 E_H–pH diagrams for the aqueous-phase reductive precipitation of gold by Sn^{2+} (left) and Fe^{2+} (right)

Purple of Cassius

When $SnCl_2$ is used, a purple colloid or precipitate forms, depending on the amount of gold present. Although knowledge and use of the precipitate dates to Egyptian records during the Roman-Greco times nearly 2,000 years ago, it is named purple of Cassius after Andreas Cassius, who used it as a pigment for making ruby-colored glass and porcelain during the late 1600s (Hunt 1976; Habashi 2016). The electrochemistry has since become well known:

Anodic reduction: $Au^{3+} + 3e^- = Au^o$ **(EQ 17)**

Cathodic oxidation: $Sn^{2+} = Sn^{4+} + 2e^-$ **(EQ 18)**

Resulting gold is nano-sized and adsorbs on colloidal tin dioxide (SnO_2) which forms when the stannic (Sn^{4+}) hydrolizes. The two precipitates therefore coagulate and effectively yield a nanocomposite with an apparent stoichiometry of $Au_2(SnO_2)_3$.

The process is depicted by the E_H–pH diagram in Figure 6 at the left with the following concentrations: 5 mM Au^{3+}, 50 mM Sn^{2+}, and 120 mM Cl^-, as studied by Tarozaite et al. (2006). Clearly, the best conditions require a pH of < 1 so that Sn^{2+} is dissolved as $SnCl^+$ and oxidizes to Sn^{4+} (Reaction 18) and then precipitates SnO_2 at a potential near –0.2 V. However, in order for Au^o to form from $AuCl_4^-$ solutions, reduction to $AuCl_2^-$ must first occur at 1.4 V. In this regard, Au^o does not form until the potential reaches approximately 1.05 V; however, this still creates a significant overpotential ($\Delta E = 1.25$ V) to drive the overall redox reaction.

Green Copperas

Ferrous sulfate ($FeSO_4$) is a teal-colored compound that has been referred to since ancient times as both green vitriol and green copperas (Gee 1920). When it is dissolved in solution and added to $AuCl_4^-$, a dark brown precipitate of Au^o forms (Hoke 1982). This gold precipitation saw significant use for recovery in the Plattner chlorination/leach process in the mid-1800s prior to cyanidation taking over the gold mining industry (Marsden and House 2006). Today, because its redox chemistry is well understood, the technology is used in gold recycling, refining, and electroless plating as well as the making of nanoparticles, nanowires, microcircuits, and mirror/optical coatings:

Anodic reduction: (See Equation 17)

Cathodic oxidation: $Fe^{2+} = Fe^{3+} + e^-$ **(EQ 19)**

These half-cell reactions are depicted by the E_H–pH diagram on the right side of Figure 6 at 0.01 M Au^{3+}, 0.01 M Fe^{2+}, and 0.5 M Cl^-. These concentrations encompass the range used in the literature (Parinayok et al. 2011; Wojnicki et al. 2015). In this case, the pH is kept below 2 and the potential difference of the Fe^{2+}/Fe^{3+} redox couple at ~0.75 V and the $AuCl_2^-/Au^o$ redox couple at ~1.05 V is low ($\Delta E = 0.3$ V), suggesting that the redox reaction will likely be chemically controlled.

Case Study 3—Organic Reduction of Gold

Gold and other precious metals can also be reduced with several organic reductants (Newman and Blanchard 2006). Perhaps the most commonly used are oxalic acid ($C_2H_2O_4$) and citric acid ($C_6H_8O_7$), which are the focus for this case study; however, there are a host of other organics that can also be used: formate, ascorbate, formaldehyde, ethylenediaminetetraacetic acid (EDTA), glutarate, acetone, alcohols, amines, and sugars, to name a few. It is understood that some organics are considered ionic because they speciate depending on

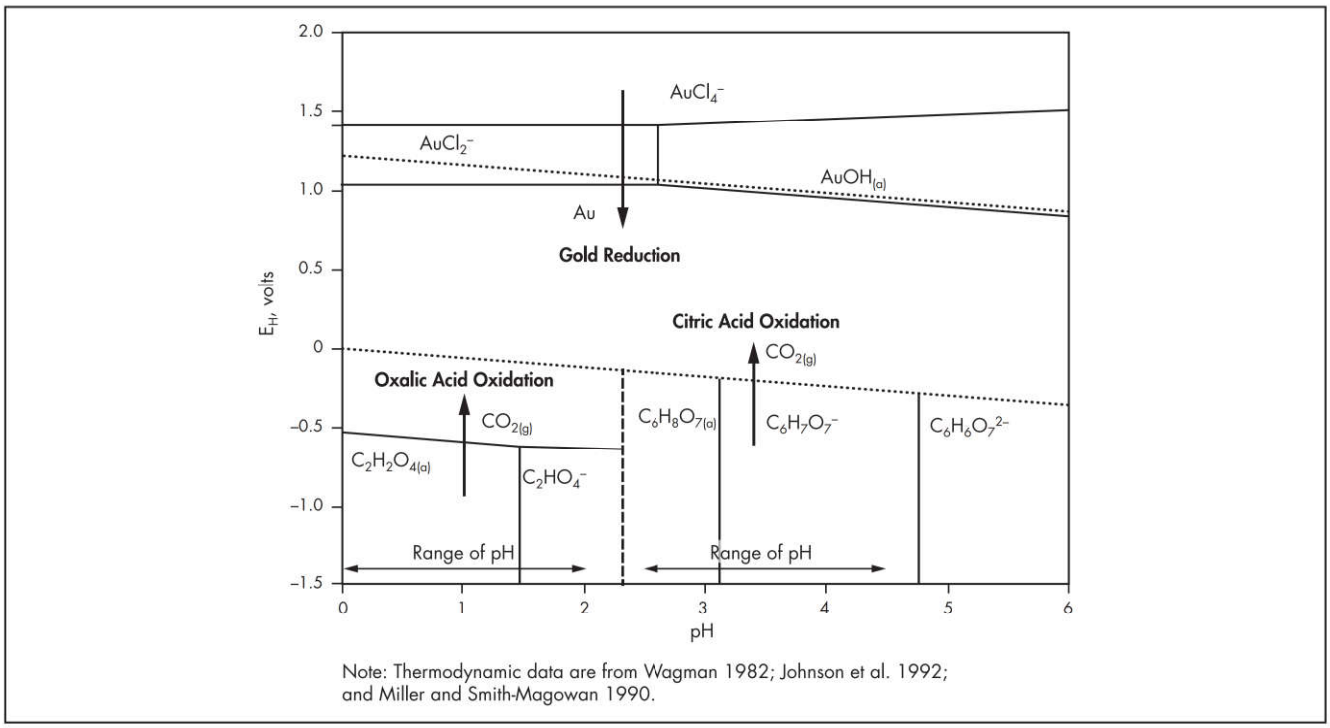

Figure 7 E_H–pH diagram for the aqueous-phase reductive precipitation of gold by oxalic acid and hydrogen oxalate (left) and citric acid, dihydrogen citrate, and monohydrogen citrate (right)

the pH, even if one of the species is uncharged. For example, oxalic acid and citric acid are neutral but, when fully unprotonated, become ionized and are referred to as oxalate and citrate, respectively. Other organics are nonionic because they are neither an acid nor a base (e.g., a polyol such as glucose sugar) and therefore do not normally protonate or hydroxylate.

Oxalic Acid

Oxalate, ferrous, and stannous ions are likely the most common reductants used for the ionic reductive precipitation of gold. Oxalate is predominantly used in refining and recycling, often as a polishing step, to produce high-purity gold due to its selectivity (Hoke 1982; Feather et al. 1997). It has also seen some use in making various nanostructures (Navaladian et al. 2007; Al-Thabaiti et al. 2015). It is favored because its redox chemistry is simple, yielding carbon dioxide (CO_2) gas as the only additional product:

Anodic reduction: (See Equation 17)

Cathodic oxidation: $C_2O_4^{2-} = 2CO_2 + 2e^-$ **(EQ 20)**

Because the CO_2 gas evolves off and gold solid precipitates out, the reaction can feasibly go to completion with high efficiency. However, it is also important to note that oxalate is not a true organic because it lacks C-H bonds, but it does behave is if it were.

On the left side of Figure 7, the E_H–pH diagram for the oxalate system is illustrated assuming Au = 0.01 M, Cl = 0.5 M, $C_2H_2O_4$ = 0.1 M, and P_{CO2} = 0.01 atm. As indicated, oxalic acid ($C_2H_2O_4$) and hydrogen oxalate ($C_2HO_4^-$) oxidize under acidic conditions less than pH 2.5 near –0.55 V at pH 0 and –0.65 V at pH 2.5. With the Au° anodic reaction occurring at ~1.05 V, a huge overpotential (ΔE) between 1.6 and 1.7 V results, depending on the pH. This large overpotential is a great example of the value of using organic reductants.

Citric Acid

Citric acid ($C_6H_8O_7$) deprotonates to citrate ($C_6H_5O_7^{3-}$) through two species: dihydrogen citrate ($C_6H_7O_7^-$) and monohydrogen citrate ($C_6H_6O_7^{2-}$). It is currently being used to prepare nanosized gold particles and wires, which require special chemicals, called stabilizers, to help control their size, shape, and growth direction. Example stabilizers include but are certainly not limited to gelatin, polyvinyl pyrrolidone, polyvinyl alcohol and acetate, polyethylene glycol, polyethyleneimine, polyamidoamine, polydithiafulvene, and chitosan (Dzimitrowicz et al. 2015; Ayoub et al. 2016). Turkevich et al. (1951) pioneered the fundamental study about the nucleation and growth of nano gold using citrate to produce nearmonosized particles. Since then, a plethora of research (Wuithschick et al. 2015) confirmed the redox chemistry:

Anodic reduction: (See Equation 17)

Cathodic oxidation:

$$C_6H_5O_7^{3-} + 5H_2O = 6CO_2 + 15H^+ + 18e^- \quad \textbf{(EQ 21)}$$

However, research efforts have shown that the reactions follow a multistep process and Reaction 21 may not go to completion, depending on how much citrate is added relative to the initial gold concentration (i.e., at, above, or below stoichiometry):

$$C_6H_5O_7^{3-} + 4H_2O = 4.5CO_2 + 10H^+ + 13e^- + CH_2O + \tfrac{1}{2}HCOOH \quad \textbf{(EQ 22)}$$

$$C_6H_5O_7^{3-} = 2CO_2 + H^+ + 2e^- + C_5H_4O_5^{2-} \quad \textbf{(EQ 23)}$$

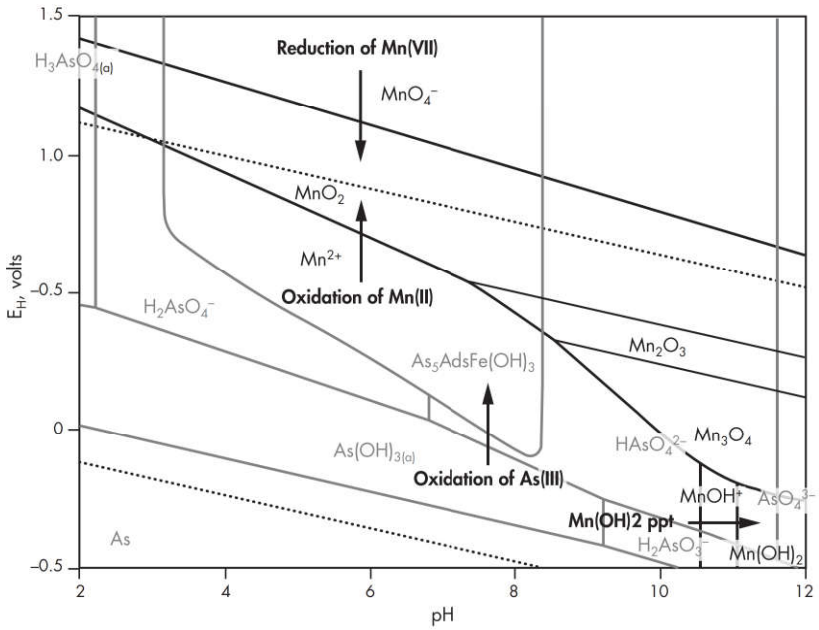

Note: Thermodynamic data are from Wagman 1982.

Figure 8 E_H–pH diagram for the aqueous-phase oxidative precipitation of Mn^{2+} (manganous) and As^{3+} (arsenite as $As(OH)_3$) with MnO_4^- (permanganate)

where, in Reaction 22, CH_2O is acetone and HCOOH is formic acid (Leng et al. 2015); and, in Reaction 23, $C_5H_4O_5^{2-}$ is 3-ketoglutarate (Verma et al. 2014). Acetone, formic acid, and glutarate are also reductants but cannot react further if all $AuCl_4^-$ was already consumed.

Figure 7 also reveals, at the right, the E_H–pH diagram for the citrate system, assuming Au = 0.005 M, Cl = 0.12 M, $C_6H_8O_7$ = 0.1 M, and P_{CO2} = 0.01 atm. As indicated, citric acid ($C_6H_8O_7$), dihydrogen citrate ($C_6H_7O_7^-$), and monohydrogen citrate ($C_6H_6O_7^{2-}$) oxidize under acidic conditions less than pH 6 and essentially at the same potentials as hydrogen evolution for water. Under these conditions, before converting to Au°, $AuCl_4^-$ will first reduce to aqueous AuOH (pH 2.5–6), primarily at the same potentials as oxygen evolution for water. Consequently, the potential difference will not be as large (ΔE = 1.2 V) as for oxalate; however, H_2 gas is not evolved, so side reactions with citrate in this regard are avoided (e.g., compare to the case study on nickel electroless plating). The best pH range for producing nanosized gold by citric acid reductive precipitation is near pH 3 and for maximizing precipitate is near pH 5.

Case Study 4—Oxidation of ARD Species

Acid rock drainage (ARD) refers to water that reacts with oxygen and sulfide-bearing rock, resulting in an acidic discharge due to the formation of sulfuric acid (H_2SO_4). Because of the acidity as well as the types of sulfide minerals involved, many metals are also solubilized including but not limited to those that are primary to, for example, the Berkeley pit lake in Butte, Montana (United States): Al, As, Cd, Cu, Fe, K, Mg, Mn, Na, and Zn (Davis and Ashenberg 1989). ARD treatment by lime (CaO) addition raises the pH and causes many of the metals to undergo hydrolytic precipitation (Zick et al. 2004); however, two stages are often needed to prevent metals from resolubilizing (Huang et al. 2005). Furthermore, to be effectively remediated, other metals must be oxidized (Twidwell and McCloskey 2011) and/or treated at high pH levels (Freitas et al. 2013), as is the situation for As^{3+} and Mn^{2+}, which are the subject of this case study. In this regard, their oxidation by permanganate (MnO_4^-) is presented and discussed:

Anodic reduction:

$$MnO_4^- + 4H^+ + 3e^- = MnO_2 + 2H_2O \quad \textbf{(EQ 24)}$$

Cathodic oxidation:

$$As(OH)_3 + H_2O = HAsO_4^{2-} + 4H^+ + 2e^- \quad \textbf{(EQ 25)}$$

$$Mn^{2+} + 2H_2O = MnO_2 + 4H^+ + 2e^- \quad \textbf{(EQ 26)}$$

$$Fe^{2+} + 3H_2O = Fe(OH)_3 + 3H^+ + e^- \quad \textbf{(EQ 27)}$$

According to Reaction 24, permanganate (MnO_4^-) will reduce to manganic oxide (MnO_2) and thereby oxidize arsenite (as $As(OH)_3$) to arsenate (as $HAsO_4^{2-}$) per Reaction 25, and manganous ion (Mn^{2+}) to manganic oxide (MnO_2) per Reaction 26. Ferrous (Fe^{2+}) oxidation to ferrihydrite ($Fe(OH)_3$) is included as Reaction 27 because resulting arsenate must adsorb at its surface to be remediated. These reactions are depicted by the E_H–pH diagram in Figure 8, which was created using approximate total concentrations for each metal found at 100-m depth in the Berkeley pit lake ARD: As = 1.0 ppm, Mn = 200 ppm, and Fe = 1,000 ppm (Davis and Ashenberg 1989).

Arsenic Remediation

Adsorbed As^{5+} (as arsenate) is labeled "$As_5AdsFe(OH)_3$" in Figure 8 and is shown to occur between pH 3 and 9 where the As^{5+} concentration in solution is less than 0.1 ppm and where the Fe:As mole ratio in solution is at least 10:1. The Drinking Water Standard for arsenic of 0.01 ppm (EPA 2012) is met between pH 4 and 7 and, according to this thermodynamic

model, is maximum between pH 5 and 6. Using the average at pH 5.5, Reaction 24 for permanganate will occur at a potential near 1.15 V. Because Reaction 25 for arsenic occurs at a potential near 0.15 V, a strong potential difference ($\Delta E = 1.0$ V) between the two half-cell reactions is observed, suggesting that the overall redox reaction will be mass-transfer/diffusion controlled. Although not depicted for clarity purposes, ferrihydrite does not form at this pH level until approximately 0.2 V is exceeded, and while arsenate adsorption will occur at this point, its concentration will not go below 0.1 ppm until a potential near 0.35 V is reached.

Manganese Remediation

The Mn^{2+} stability region in Figure 8 denotes the E_H–pH conditions where its concentration falls below the manganese National Secondary Drinking Water Regulation of 0.05 ppm (EPA 2012). Its ionic precipitation as $Mn(OH)_2$ is also shown to occur at pH 11. While attainable, it is not cost-effective due to the amount of lime that would be needed; furthermore, the resulting water would have to be treated even more to meet the pH-8.5 requirements for discharge. Hence, its remediation is best accomplished through aqueous-phase oxidative precipitation. Considering pH 5.5 per the arsenic discussions, Reaction 26 for manganous ion oxidation occurs near 0.75 V, and with Reaction 24 occurring at 1.15 V, a moderate potential difference ($\Delta E = 0.4$ V) will occur. Thus, the overall reaction is also expected to be mass-transfer/diffusion controlled, albeit on the threshold of being chemical reaction control. Although the process is known to work, the only issue is that remediation is dependent on precision: too much or not enough permanganate will still leave manganese in solution. In this regard, the preferred oxidant is nonionic hydrogen peroxide (H_2O_2).

OTHER HYDROMETALLURGICAL PROCESSES

In this section, other examples of aqueous-phase precipitation processes are given but are not illustrated with E_H–pH diagrams. Although there is an abundance of other examples, only five current industrial and research examples are emphasized, with minor discussions given as needed. While the same concepts apply, it is only necessary to show applications with other types of redox reagents and/or metals. This is made simpler by showing only the overall redox reactions instead of half-cell reactions.

Tollens' Process

Tollens' process is an electroless plating technique commonly applied to coating glass for optical purposes. It is used for making silver mirrors and thus referred to as silvering (Antonello et al. 2012). Because the reaction is similar to nonionic organic reduction, it is also being used to make nanoparticles, nanowires, and microcircuits (Purdy and Muscat 2016). The reaction is frequently used as a demonstration in chemistry labs around the world to coat the inside of flasks or the surface of glass slides:

$$2Ag(NH_3)_2^+ + 3OH^- + RCHO = 2Ag^\circ + RCOO^- + 4NH_3 + 2H_2O \quad \textbf{(EQ 28)}$$

where RCHO and $RCOO^-$ are usually aldehydes and carboxylates such as glocose and gluconic acid, respectively.

Se/Te Removal Process

Because sulfate is considered the most stable form of sulfur, sulfur-containing compounds with lower oxidation states than sulfate tend to be excellent reductants. In this regard, sulfurous acid (H_2SO_3) is used to remove selenite (SeO_3^{2-}) and tellurite (TeO_3^{2-}) from copper-bearing leach solutions prior to copper electrowinning, particularly in platinum group metal refineries (Lottering et al. 2012):

$$2Cu^{2+} + SeO_3^{2-} + 4H_2SO_3 + H_2O = Cu_2Se^\circ + 4H_2SO_4 + 2H^+ \quad \textbf{(EQ 29)}$$

where the Cu_2Se° is an alloy that is filtered and sold. TeO_3^{2-} reacts the same way and consequently is sold with the Cu_2Se°. High temperatures may be needed for both reactions, particularly if both Se and Te are present in higher oxidation states.

Sherritt Gordon Process

Following ammoniacal leaching of Ni-Co sulfide concentrates, a typical leach solution at the Fort Saskatchewan operations in Alberta, Canada, would contain ~100 g/L free ammonia (NH_3), 5–10 g/L sulfur mostly as thiosulfate ($S_2O_3^{2-}$), 40–50 g/L Ni^{2+}, 0.7–1 g/L Co^{2+}, and 5–10 g/L Cu^{2+} (Wadsworth 1987). As soon as the free ammonia was thermally removed by steam injection, the thiosulfate would disproportionate into sulfide and sulfate, with the former causing the cuprous (Cu^{2+}) to precipitate:

$$Cu^{2+} + S_2O_3^{2-} + H_2O = CuS + SO_4^{2-} + 2H^+ \quad \textbf{(EQ 30)}$$

In this case, it is the change in state of the sulfur that leads to the metal being ionically precipitated. Importantly, dithionite ($S_2O_4^{2-}$) and other sulfoxy compounds are known to cause reductive precipitation of cupric to metallic copper but is not observed here, presumably because the chemical environments are distinctly different.

Cyanide Destruction Processes

Similarly, the oxidation of cyanocomplexes can also lead to metal precipitation (Young et al. 2001). This includes reactions with several dissolved oxidants including but not limited to hydrogen peroxide (H_2O_2), Caro's acid (H_2O_5), bleach/hypochlorite (OCl^-), bisulfite (HSO_3^-), and metabisulfate ($S_2O_7^{2-}$). Because the reactions are similar, only that involving hypochlorite is depicted:

$$M(CN)_4^{-2} + 4OCl^- + 2OH^- = 4OCN^- + 4Cl^- + M(OH)_2 \quad \textbf{(EQ 31)}$$

where, in this case, M represents a common divalent weak-acid-dissociable cyanide such as Zn^{2+} and Cd^{2+}, for example. It is understood that additional hypochlorite will form carbonate (CO_3^{2-}) and either nitrite (NO_2^-) or nitrate (NO_3^-). This particular process also works for free cyanide and thiocyanate but not strong-acid-dissociable cyanide. Furthermore, it is not normally used on a large scale but is commonly used for cyanide destruction in most chemical and research labs.

ARD Schwertmannite Process

Schwertmannite is a solid solution found as a precipitate in ARD systems. It has an approximate stoichiometry of $(Fe_8O_8(OH)_{4.8}(SO_4)_{1.6})$ and can be synthesized by contacting ARD with hydrogen peroxide (H_2O_2):

$$8Fe^{2+} + 1.6SO_4^{2-} + 2H_2O_2 + 8.8H_2O = Fe_8O_8(OH)_{4.8}(SO_4)_{1.6} + 12.8H^+ \quad \textbf{(EQ 32)}$$

As with permanganate, hydrogen peroxide oxidizes ferrous (Fe^{2+}) to ferric (Fe^{3+}) to induce the precipitation. Furthermore, arsenite (AsO_3^{3-}) will also oxidize to arsenate (AsO_4^{3-}), which can then substitute for sulfate in the compound (Liu et al. 2015).

REFERENCES

Al-Thabaiti, S.A., Obaid, A.Y., and Khan, Z. 2015. Gold nanocomposites: Kinetic, mechanistic and structural effects of reducing agents on the morphology, *Can. Chem. Trans.* 3(1):12–28.

Antonello, A., Jia, B., He, Z., Buso, D., Perotto, G., Brigo, L., Brusatin, G., Guglielmi, M., Gu, M., and Martucci, A. 2012. Optimized electroless silver coating for optical and plasmonic applications. *Plasmonics* 7.

Ayoub, A.H., Safadi, N., Inibtawi, M., and Shadafny, S. 2016. Formulation of small size gold nano-particles stabilized with novel polyethylene glycol (PEG)-n-acetyl cysteine (NAC) conjugate, *J. Chem.* 5(4):16–21.

Brenner, A., and Riddell, G.E. 1946. Nickel coating on steel by chemical reduction. *J. Res. Nat. Bur. Std.* 37(1):31–34.

Davis, A., and Ashenberg, D. 1989. Aqueous geochemistry of the Berkeley Pit, Butte, Montana, U.S.A. *Appl. Geochem.* 4:23–36.

Dzimitrowicz, A., Jamroz, P., Greda, K., Nowak, P., Nyk, M., and Pohl, P. 2015. The influence of stabilizers on the production of gold nanoparticles by direct current atmospheric pressure glow microdischarge generated in contact with liquid flowing cathode. *J. Nanopart. Res.* 17(4):185–192.

EPA (U.S. Environmental Protection Agency). 2012. *2012 Edition of the Drinking Water Standards and Health Advisories.* EPA 822-S-12-001. Washington, DC: EPA.

Feather, A., Sole, K.C., and Bryson, L.J. 1997. Gold refining by solvent extraction—The Minataur™ process. *J. SAIMM* 105(July/August):169–173.

Freitas, R.M., Perilli, T.A.G., and Ladeira, A.C.Q. 2013. Oxidative precipitation of manganese from acid mine drainage by potassium permanganate. *J. Chem.* Vol. 2013.

Gee, G.E. 1920. *Recovering Precious Metals from Waste Liquid Residues: A Complete Workshop Treatise Containing Practical Working Directions for the Recovery of Gold, Silver and Platinum from Every Description of Waste Liquids in the Jewellery, Photographic, Process Workers, and Electroplating Trades.* New York: Spon and Chamberlain.

Habashi, F. 1999. *A Textbook of Hydrometallurgy*. Saint Foy, QC: Métallurgie Extractive Québec.

Habashi, F. 2016. Purple of Cassius: Nano gold or colloidal gold? *Eur. Chem. Bull.* 5(10):416–419.

Hoke, C.M. 1982. *Refining Precious Metal Wastes: Gold, Silver, Platinum Metals; A Handbook for the Jeweler, Dentist, and Small Refiner*. New York: Metallurgical Publishing.

House, C.I., and Kelsall, G.H. 1984. Potential–pH diagrams for the Sn/H_2O-Cl system. *Electrochim. Acta* 29(10):1495–1464.

Huang, H-H. 2018. *StabCal: Stability Calculation for Aqueous System, Programs and User Manual.* Butte, MT: University of Montana, Metallurgical and Materials Engineering.

Huang, H.H., Twidwell, L.G., Anderson, C.G., and Young, C.A. 2005. Chemical titration simulation—An equilibrium calculation approach. In *Proceedings of the International Symposium on Computational Analysis in Hydrometallurgy*. Edited by D.G. Dixon and M.J. Dry. Montreal, QC: Canadian Institute of Mining, Metallurgy and Petroleum.

Hunt, L.B. 1976. The true story of purple of Cassius: The birth of gold-based glass and enamel colours. *Gold Bull.* 9(4):134–139.

Johnson, J.W., Oelkers, E.H., and Helgeson, H.C. 1992. SUPCRT92: A software package for calculating the standard molal thermodynamic properties of minerals, gases, aqueous species, and reactions from 1 to 5000 bar and 0 to 1000°C. *Comp. Geosci.* 16(7):899–947.

Leng, W., Pati, P., and Vikesland, P.J. 2015. Room temperature seed mediated growth of gold nanoparticles: Mechanistic investigations and life cycle assessment. *Environ. Sci. Nano* 2(5):440–453.

Liu, F., Zhou, J., Zhang, S., Liu, L., Zhou, L., and Fan, W. 2015. Schwertmannite synthesis through ferrous ion chemical oxidation under different H_2O_2 supply rates and its removal efficiency for arsenic from contaminated groundwater. *PLOS One* 10(9):e0138891.

Lottering, C., Eksteen, J.J., and Steenekamp, N. 2012. Precipitation of rhodium from a copper sulphate leach solution in the selenium/tellurium removal section of a base metal refinery. *J. SAIMM* 112(April):287–94.

Mallory, G.O. 1990. The fundamental aspects of electroless nickel plating. In *Electroless Plating: Fundamentals and Applications.* Edited by G.O. Mallory and B.J. Hajdu. New York: American Electroplaters and Surface Finishing Society. pp. 1–56.

Mallory, G.O., and Hajdu, B.J., eds. 1990. *Electroless Plating: Fundamentals and Applications.* New York: American Electroplaters and Surface Finishing Society.

Marsden, J.O., and House, C.I. 2006. *The Chemistry of Gold Extraction.* Littleton, CO: SME.

Miller, S.L., and Smith-Magowan, D. 1990. The thermodynamics of the Krebs cycle and related compounds, *J. Phys. Ref. Data* 19(4):1049–1073.

Navaladian, S., Janet, C.., Viswanathan, B., Varadarajan, T.K., and Viswanath, R.P. 2007. A facile room-temperature synthesis of gold nanowires by oxalate reduction method. *J. Phys. Chem.* 111(38):14150–14156.

Newman, J.D., and Blanchard, G.J. 2006. Formation of gold nanoparticles using amine reducing reagents. *Langmuir* 22(13):5882–5887.

Parinayok, P., Yamashita, M., Yonezu, K., Ohashi, H., Watanabe, K., Okaue, Y., and Yokoyama, T. 2011. Interaction of Au(III) and Pt(IV) complex ions with Fe(II) ions as a scavenging and a reducing agent: A basic study on the recovery of Au and Pt by a chemical method. *J. Colloid Interface Sci.* 364(1):272−275.

Purdy, S.C., and Muscat, A.J. 2016. Coating nonfunctionalized silica spheres with a high density of discrete silver nanoparticles. *J. Nanoparticle Res.* 18(3):70–92.

Sudagar, J., Lian, J., and Sha, W. 2013. Electroless nickel, alloy, composite and nano coatings—A critical review. *J. Alloys Compd.* 571:183–204.

Tarozaite, R., Juskenas, R., Kurtinaitiene, M., Jagminiene, A., and Vaskelis, A. 2006. Gold colloids obtained by Au(III) reduction with Sn(II): Preparation and characterization. *Chemija* 17(2-3):1–6.

Turkevich, J., Stevenson, P.C., and Hillier, J. 1951. A Study of the Nucleation and Growth Processes in the Synthesis of Colloidal Gold. *Discuss. Faraday Soc.* 11:55–75.

Twidwell, L.G., and McCloskey, J.W. 2011. Removing arsenic from aqueous solution long-term product storage. *JOM* 63(8):94–110.

Verma, H.N., Singh, P., and Chavan, R.M. 2014. Gold nanoparticle: Synthesis and characterization. *Vet. World* 7(2):72–77.

Wadsworth, M.E. 1987. Leaching—Metals applications. In *Handbook of Separation Process Technology*. Edited by R.W. Rousseau. Norwich, NY: Knovel.

Wagman, D.D. 1982. *The NBS Tables of Chemical Thermodynamic Properties: Selected Values for Inorganic and C_1 and C_2 Organic Substances in SI Units.* New York; Washington, DC: American Chemical Society and American Institute of Physics for the National Bureau of Standards.

Wojnicki, M., Zabieglinska, K., and Luty-Blocho, M. 2015. Influence on experimental condition on silver nanoparticle synthesis process in aqueous solutions. *Ores Nonferrous Met.* 60(3):103–109.

Wuithschick, M., Birnbaum, A., Witte, S., Sztucki, M., Vainio, U., Pinna, N., Rademann, K., Emmerling, F., Kraehnert, R., and Polte, J. 2015. Turkevish in new robes: Key questions answered for the most common gold nanoparticle synthesis. *ACS Nano* 9(7):7052–7071.

Young, C.A., Anderson, C.G., and Twidwell, L.G., eds. 2001. *Cyanide: Social, Industrial and Economic Aspects.* Warrendale, PA: The Minerals, Metals & Materials Society.

Zick, R.L., Velegol, D.A. Jr., Hess, M.W., and Foote, M. 2004. Butte mine flooding water treatment facility: Implementation of major component of selected remedy for historic contamination at Berkeley Pit site. In *Proceedings of the Joint Conference of the 21st Annual Meeting of the American Society of Mining and Reclamation and 25th West Virginia Surface Mine Drainage Task Force Symposium*. Edited by R.I. Barnhisel. Lexington, KY: American Society of Mining and Reclamation. pp. 2079–2104.

PART 11

Pyrometallurgy